Multipolar Force Fields for Amide-I Spectroscopy from Conformational Dynamics of the Alanine Trimer

Mondal, P.; Cazade, P.-A.; Das, A.K.; Bereau, T.; Meuwly, M.

DOI
10.1021/acs.jpcb.1c05423

Publication date
2021

Document Version
Final published version

Published in
Journal of Physical Chemistry B

THE JOURNAL OF PHYSICAL CHEMISTRY B
A JOURNAL OF THE AMERICAN CHEMICAL SOCIETY

pubs.acs.org/JPCB

Article

Multipolar Force Fields for Amide-I Spectroscopy from Conformational Dynamics of the Alanine Trimer

Padmabati Mondal,* Pierre-André Cazade, Akshaya K. Das, Tristan Bereau, and Markus Meuwly*

Cite This: *J. Phys. Chem. B* 2021, 125, 10928–10938

Read Online

ACCESS | Metrics & More | Article Recommendations | Supporting Information

ABSTRACT: The dynamics and spectroscopy of *N*-methyl-acetamide (NMA) and trialanine in solution are characterized from molecular dynamics simulations using different energy functions, including a conventional point charge (PC)-based force field, one based on a multipolar (MTP) representation of the electrostatics, and a semiempirical DFT method. For the 1D infrared spectra, the frequency splitting between the two amide-I groups is 10 cm^{-1} from the PC, 13 cm^{-1} from the MTP, and 47 cm^{-1} from self-consistent charge density functional tight-binding (SCC-DFTB) simulations, compared with 25 cm^{-1} from experiment. The frequency trajectory required for the frequency fluctuation correlation function (FFCF) is determined from individual normal mode (INM) and full normal mode (FNM) analyses of the amide-I vibrations. The spectroscopy, time-zero magnitude of the FFCF $C(t = 0)$, and the static component Δ_0^2 from simulations using MTP and analysis based on FNM are all consistent with experiments for $(Ala)_3$. Contrary to this, for the analysis excluding mode−mode coupling (INM), the FFCF decays to zero too rapidly and for simulations with a PC-based force field, the Δ_0^2 is too small by a factor of two compared with experiments. Simulations with SCC-DFTB agree better with experiment for these observables than those from PC-based simulations. The conformational ensemble sampled from simulations using PCs is consistent with the literature (including P_{II}, β, α_R, and α_L), whereas that covered by the MTP-based simulations is dominated by P_{II} with some contributions from β and α_R. This agrees with and confirms recently reported Bayesian-refined populations based on 1D infrared experiments. FNM analysis together with a MTP representation provides a meaningful model to correctly describe the dynamics of hydrated trialanine.

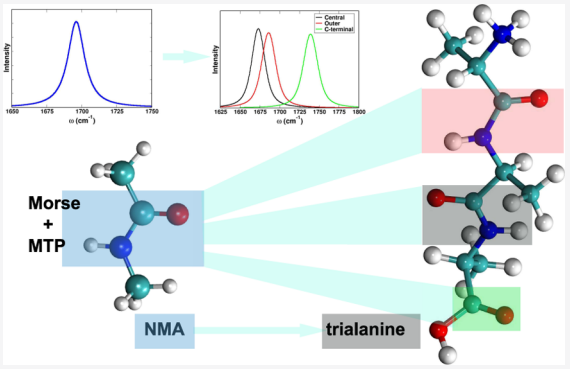

INTRODUCTION

Ultrafast infrared (IR) spectroscopy is a powerful tool to characterize the solvent dynamics around chromophores on the pico- and sub-picosecond time scale. It has also been proven to be a promising tool for studying the structure and dynamics of proteins, including protein-folding and protein−ligand binding.[1−7] The amide-I mode is suitable to probe the structural dynamics and the conformational ensemble of a solvated molecule, peptide, or protein.[1,8] Other suitable vibrational labels[9,10] that absorb in the spectroscopic window between ∼ 1700 and ∼ 2800 cm^{-1} are cyanophenylalanine,[11] nitrile-derivatized amino acids,[12] the sulfhydryl band of cysteines,[13] deuterated carbons,[14] non-natural labels consisting of metal-tricarbonyl modified with a $-(CH_2)_n-$ linker,[15] nitrile labels,[3] cyano[16] groups, SCN,[17] or cyanamide.[18] Contrary to these other probes, the amide-I band characterizes the inherent dynamics of the system because it does not require mutation or chemical modification of the molecule considered.

N-methyl acetamide (NMA) is a typical model system for experimental[19−23] and computational[24−27] studies because it is also the fundamental building block to study longer peptides and proteins. In going from a mono- to a poly-peptide, one essentially moves from NMA to alanine dipeptide, to trialanine, and to longer alanine chains. Therefore, to develop and validate force fields for the amide probe and to apply them to longer polypeptides chains, starting from NMA is a meaningful choice. This also allows one to assess the transferability of the force fields from NMA by using them for polypeptides and comparing the results with experimental data.

Two-dimensional infrared (2D-IR) spectroscopy provides quantitative information about the solvent structure and dynamics surrounding a solute.[10] Such techniques are particularly useful to measure the fast (picosecond) dynamics in condensed-phase systems. The coupling between inter- and intramolecular degrees of freedom—such as the hydrogen bonding network in solution or the conformational dynamics of biological macromolecules—can be investigated by

Received: June 20, 2021
Published: September 24, 2021

https://doi.org/10.1021/acs.jpcb.1c05423
J. Phys. Chem. B 2021, 125, 10928−10938

monitoring the fluctuation of a fundamental vibrational frequency, which is the amide-I mode in the present work. Computationally, this information is accessible from either instantaneous normal modes (NMs),[5,24,28] the solution of a reduced-dimensional nuclear Schrödinger equation,[29,30] or from spectroscopic maps.[23] This frequency trajectory [$\omega(t)$ or $\nu(t)$ for harmonic or anharmonic vibrations, respectively] is then used to determine the frequency fluctuation correlation function (FFCF) which can be directly compared with experimental measurements.

The linear and non-linear vibrational spectroscopy and conformational dynamics of trialanine in solution have been investigated from both, experiments and computations.[31−41] Computationally, a quantum-classical description of the amide-I vibrational spectrum of trialanine in D_2O probed different approximations typically made in determining the vibrational line shapes.[38] A combined experimental and molecular dynamics (MD) study using non-linear time-resolved spectroscopy on trialanine found conformational heterogeneity of the peptide.[32] Peptide conformational ensembles were also studied for trialanine using 2D IR and NMR spectroscopies.[39−41] 2D IR studies probed the subpicosecond dynamics[33] and with isotopically labelled $(Ala)_3$, the dipole−dipole coupling strength was determined.[35] Including such couplings is often carried out in models based on spectroscopic maps. In the present work, NMs are determined from "independent normal mode" (INM) and from "full normal mode" (FNM) analyses which allow coupling of two or several amide-I modes.

The present work is structured as follows. First, the methods used are introduced. Then, the spectroscopy and dynamics of solvated and deuterated NMA is analyzed for a flexible solute. Next, the spectroscopy and structural dynamics of trialanine are discussed. Finally, conclusions are drawn.

COMPUTATIONAL METHODS

Molecular Dynamics Simulations. MD simulations were carried out for *N*-deuterated *N*-methylacetamide (NMAD, see Figure 1) and trialanine $(Ala)_3$ in a periodic cubic box of deuterated TIP3P[42] water molecules. The box size was 30^3 Å^3, and the system consisted of one solute molecule surrounded by 882 water molecules (for NMAD) and 795 water molecules (for $(Ala)_3$), respectively. $(Ala)_3$ was fully deuterated, and the positively charged species (i.e., "cationic" with ND_3^+ and COOD termini) was investigated.[31,41] To neutralize the simulation system, one chloride ion was added and constrained in one corner of the simulation system during MD simulations.

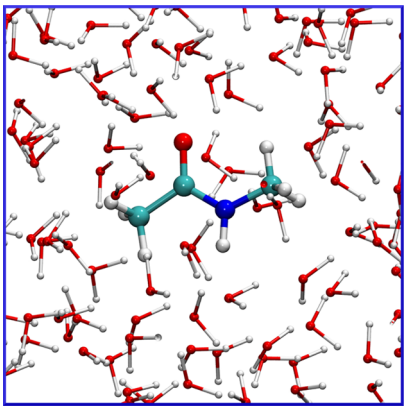

Figure 1. NMAD solvated in D_2O. Only part of the water box is shown. Atom color code: carbon (cyan), oxygen (red), nitrogen (blue) , and hydrogen (white).

All MD simulations were performed with the CHARMM program[43] with provision for multipolar (MTP) interactions.[44,45] Parameters for NMA are based on CGenFF[46] unless stated otherwise and described in more detail in ref 24. Electrostatic interactions were treated using Particle-Mesh Ewald[47] with a grid-size spacing of 1 Å, characteristic reciprocal length κ = 0.43 Å^{-1}, and interpolation order 4 for long-range electrostatics. For the Lennard-Jones (LJ) interactions, a 12 Å cut-off and 10 Å switching were used. The simulations were performed at T = 300 K, and all bonds involving hydrogen atoms were constrained via the SHAKE algorithm.[48] The time step was Δt = 0.5 fs, and snapshots were collected every 5 fs time steps.

Mixed QM/MM simulations were carried out using self-consistent charge density functional tight-binding (SCC-DFTB),[49] as implemented in CHARMM.[50] In these simulations, the entire solute (NMAD or $(Ala)_3$) was treated with SCC-DFTB, whereas all water molecules and the ion (for the solvated $(Ala)_3$ system) were treated by MM. Van der Waals parameters on the solute were those of the CHARMM force field. First, the system was minimized and heated to 300 K. An *NVT* simulation was carried out at 300 K using the velocity Verlet integrator with a (shorter) time step of Δt = 0.25 fs for 5 ns. Again, all bonds involving hydrogen atoms were constrained using SHAKE,[48] and the treatment of the nonbonded interactions was the same as that for the PC and MTP simulations described above.

Force Fields for Flexible NMA. Two different electrostatic models for NMA are used in this work. The first one uses point charges (PCs) based on the CGenFF force field. The second model is the multipolar MTPS representation including atomic multipoles up to quadrupoles for the entire NMAD molecule taken from ref 24 and also given in Table S1 in Supporting Information. The force field parameters for the CO bond are based on ab initio calculations at the MP2/6-31G** level and are readjusted to reproduce the gas phase amide-I frequency. The Morse parameters are D_e = 141.67 kcal mol^{-1}, β = 2.11 Å^{-1}, and r_{eq} = 1.23 Å.

The parametrization for $(Ala)_3$ uses the CGenFF force field[51] except for the CO-stretch potential which is the same Morse function used for the −CO group of NMAD, the multipoles on the C-terminal CO atoms, and outer and central [CONH] atoms which were also used for [CONH] group of NMAD. The MTP model used here is also the MTPS model, and the parameters are given in Table S2.

Frequency Fluctuation Correlation Function and 1D IR Spectrum. The FFCF, $C(t)$, is obtained from the frequency trajectory $\omega(t)$ according to

$$C(t) = \langle \delta\omega(t_0)\delta\omega(t_0 + t)\rangle_{t_0} = \langle (\omega(t_0) - \bar{\omega})(\omega(t_0 + t) - \bar{\omega})\rangle_{t_0} \quad (1)$$

where $\omega(t_0)$ is the instantaneous frequency at time t_0 and $\bar{\omega}$ is the average frequency and thereby $\delta\omega(t_0)$ refers to the frequency fluctuation at time t_0. The instantaneous frequencies $\omega(t)$ are obtained from NM calculations. For each snapshot of the trajectory, the structure of the solute (here NMAD and $(Ala)_3$) is minimized while keeping the solvent frozen. Frequencies are calculated using two different approaches referred to as FNM and INM analysis methods. For FNM, NM

https://doi.org/10.1021/acs.jpcb.1c05423
J. Phys. Chem. B 2021, 125, 10928−10938

analysis is carried out for the entire solute. Such an approach includes both the frequencies of the labels ("site energies") and the couplings between them. On the other hand, INM refers to the NM analysis of the independent amide modes of trialanine while keeping everything except the [CONH] group fixed and therefore neglects the couplings between the spectroscopic labels. This approach is computationally more efficient than scanning along the NM and solving the 1D or even 3D nuclear Schrödinger equation.[8,29,52]

The analysis adopted here is also reminiscent of instantaneous NMs which have been shown to perform well for the short-time dynamics in the condensed phase.[53−56] Furthermore, a direct comparison between instantaneous NMs, scanning ("scan") along the NM, and map-based frequency trajectories have been recently presented and found that "NM" and "scan" yield comparable FFCFs and 1D line shapes derived from them.[8]

The 1D and 2D response functions can be determined from the line shape function $g(t)$,[19,57] which is related to the FFCF through

$$g(t) = \int_0^t \int_0^{\tau'} d\tau' \, d\tau'' \langle \delta\omega(\tau'')\delta\omega(0)\rangle \tag{2}$$

Depending on whether or not the FFCF is fit to a parametrized form, the double integration can be carried out in closed form or needs to be carried out numerically. In the present case, the functional form fitted to is

$$C(t) = \sum_{i=1}^{n} a_i \exp(-t/\tau_i) + \Delta_0^2 \tag{3}$$

with amplitudes a_i and decay times τ_i as fitting parameters and $n_{max} = 2$ or 3 to make direct comparison with earlier work on $(Ala)_3$.[58] The a_i and τ_i are amplitudes and relaxation times, respectively, and Δ_0^2 is the static component which can differ from 0 for situations in which processes occurring on longer time scales have not equilibrated on the time scales of the relaxation times τ_i (i.e., structural heterogeneity).

RESULTS

Spectroscopy of NMAD. To validate the energy functions and analysis techniques used subsequently for $(Ala)_3$, first the spectroscopy of NMAD in D_2O from MD simulations with PCs and MTPs for flexible solute was considered. In addition, QM(SCC-DFTB)/MM simulations were also carried out. For each of the three cases, 10^6 snapshots from a 5 ns long trajectory were analyzed. For every snapshot, the frequency, $\omega(t)$, was obtained from an instantaneous NM analysis. From this, the FFCFs were determined and fitted to multi-exponential decay functions along with a static component (Δ_0^2) according to eq 3 with $n_{max} = 2$ or 3.

Figure 2 shows the FFCF for NMAD in D_2O for the simulations with the PC (red), MTP (blue), and SCC-DFTB (orange) models. The fits, using two or three time scales, respectively, are the dashed and solid green, black, and cyan lines. The fitting parameters for the FFCFs are summarized in Table 1. Figure 2 shows that for PC, MTP, and SCC-DFTB, two time scales are sufficient to represent the FFCF. Also, for the two force field models, the FFCFs decay to zero on the ~10 ps time scale, whereas that from the SCC-DFTB simulations has a static component of $\Delta_0^2 = 1.3$ ps^{-2}. As mentioned above, a finite static component is usually associated with processes that have not relaxed on the time

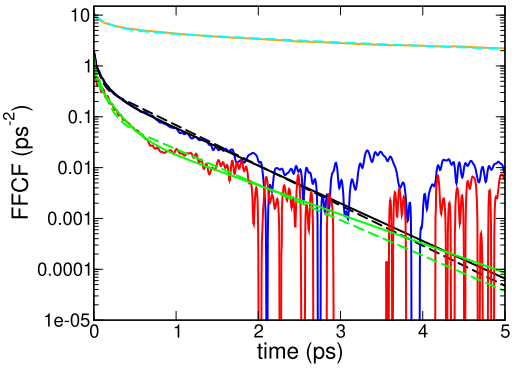

Figure 2. FFCFs for NMAD in D_2O (TIP3P) for simulations with PC (red), MTP (blue), and SCC-DFTB (orange) with flexible NMA. Green, black, and cyan lines are fits to eq 3 for the FFCFs from simulations with PC, MTP, and SCC-DFTB, respectively. Dashed lines are for fits using $n_{max} = 2$, and solid lines are for fits with $n_{max} = 3$ in eq 3.

scale of the decay time(s) of the FFCF. However, no simple explanation could be found so far.

The short time decay τ_1 for the PC and MTP models ranges from 0.02 ps to 0.08 ps, consistent with experiments (between 0.01 and 0.1 ps).[32,59] Contrary to that, simulations with SCC-DFTB yield $\tau_1 = 0.18$ ps which is at least a factor of two slower compared with what has been reported from experiments. The long time scale, τ_3, ranges from 0.55 to 0.62 ps, compared with 1.0 ps and 1.6 ps from the experiments.[32,59] Earlier MD simulations reported $\tau_3 = 0.66$ ps.[59] The SCC-DFTB simulations find a long time scale $\tau_3 = 3.2$ ps which is longer than any of the experiments. It is also worthwhile to note that a two-time scale fit of the FFCF to the frequencies from the MTP simulation is sufficient and assuming three time scales does not provide additional information. This is also found from the experiments.[59] The fits with only two time scales are preferred, and with every additional time scale, a new process is associated. For water, the sub-picosecond time scale has been associated with partial water reorientation, whereas the process on the picosecond time scale is considered to involve full water reorientation.[60]

The 1D absorption spectra are calculated from the analytical integration[5,61] of the line shape function (see eq 2) with the FFCF ($C(t)$) fit to eq 3. A phenomenological broadening for the amide-I vibration consistent with a lifetime of 0.45 ps was used.[21] The maxima of the 1D line shape for NMAD in D_2O for the PC, MTP, and SCC-DFTB models are 1705, 1695, and 1695 cm^{-1}, respectively, see Figure 3. The gas phase frequency for the amide mode of NMAD is 1717 cm^{-1}, and solvent-induced red-shifts for the PC, MTP, and SCC-DFTB models are 12, 22, and 22 cm^{-1}, respectively. This compares with an experimental solvent-induced red-shift of 85 cm^{-1}.[62] The full width at half-maximum (fwhm) of the calculated 1D absorption spectra (Figure 3) for NMAD in D_2O using the PC, MTP, and SCC-DFTB models is 12.5, 14, and 35 cm^{-1}, compared with ~20 cm^{-1} from experiments.[58]

In summary, the PC and MTP models correctly capture the short and long time scales compared with experiment with the MTP model performing somewhat better. Simulations with both force fields correctly find that the FFCFs decay to zero on the few-picosecond time scale, whereas SCC-DFTB leads to a static component which was not found in the experiments. For the 1D IR spectroscopy, all models find a solvent-induced red

https://doi.org/10.1021/acs.jpcb.1c05423
J. Phys. Chem. B 2021, 125, 10928−10938

Table 1. Parameters of Tri/bi-exponential Fit (eq 3) for MTP and PC Models and Bi-exponential Plus Static Component Fit (eq 3) for SCC-DFTB Calculations for the FFCFs of the Carbonyl Group of NMAD in D_2O for Different Models

model	a_1 [ps^{-2}]	τ_1 [ps]	a_2 [ps^{-2}]	τ_2 [ps]	a_3 [ps^{-2}]	τ_3 [ps]	Δ_0^2 [ps^{-2}]
PC	0.470	0.019	0.597	0.075	0.085	0.588	
PC (bi-exp)	0.951	0.080			0.115	0.622	
MTP	0.942	0.019	0.707	0.110	0.330	0.587	
MTP (bi-exp)	1.361	0.049			0.418	0.550	
SCC-DFTB	4.488	0.183			3.982	3.202	1.344
sim.[59]		0.06				0.66	
exp.[32]		(0.05−0.1)				1.6	
exp.[59]		0.01				1.0	

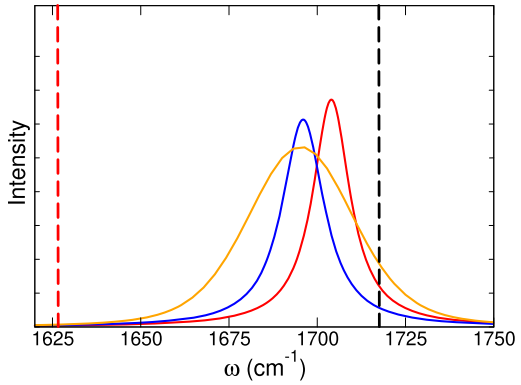

Figure 3. 1D absorption spectra of NMAD in D_2O in the region of the amide-I mode from simulations with the PC (red), MTP (blue), and the SCC-DFTB (orange) models. Experimental peaks for the amide I mode of NMAD in D_2O and in the gas phase are shown as red and black dashed vertical lines, respectively. The experimental solvent-induced red shift is 85 cm^{-1}.[62,63]

shift which, however, underestimates the experimentally reported magnitude, and the fwhm from MTP is closest to that observed experimentally.[58] These findings are also consistent with earlier work that used a frozen NMAD solute to evaluate the 1D and 2D spectroscopies.[24]

Spectroscopy and Dynamics of Trialanine. Next, the spectroscopy and dynamics of $(Ala)_3$ (see Figure 4) are

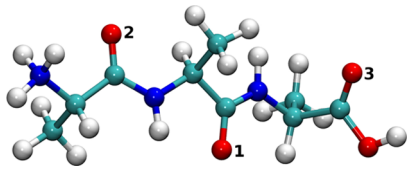

Figure 4. Structure of protonated (cationic) $(Ala)_3$.[31] The central (1), outer (2), and carboxylic (3) −CO groups are specifically labeled. Hydrogen (white), oxygen (red), nitrogen (blue), and carbon (cyan) are shown as spheres.

considered. Trialanine involves two amide-I groups (central and outer −CO) and one terminal carboxylic (COOH) group. For each interaction model, 10 ns MD simulations were performed for deuterated trialanine in deuterated water using the PC, MTP, and SCC-DFTB models (validated for NMAD in D_2O). This was preceded by 1 ns of *NPT* equilibration and further 100 ps *NVT* equilibration. The −CO(OH) group of trialanine is characteristically different from the amide −CO group. To account for this, a slightly modified Morse (β) parameter (than what has been used for C═O of NMAD in D_2O) is used for the C-terminal −CO group in the simulations and NM calculations.

Frequency Distributions. Frequencies for the central and outer amide and terminal CO(OH) are calculated using both FNM and INM analyses. The experimentally determined peak positions are at 1650, 1675, and 1725 cm^{-1} for the central, outer, and carboxylic −CO, respectively.[31] In the following, results from the FNM analysis are discussed first and then compared with those obtained from INMs, see Figure 8 and Table 2.

Figure 5A,B shows the frequency distribution for the central (black), outer (red), and terminal (green) carbonyl group from simulations with the MTP and SCC-DFTB models, respectively. The down-headed arrows of corresponding color indicate the experimental[31] peak positions of each −CO group, and the vertical dashed lines refer to the shifted experimental peak position to best overlap with the simulated data for the central −CO. This is meaningful because for the present work primarily relative positions of the absorption bands are of interest. Fine-tuning of the Morse parameters to match experimental line positions would still be possible for the PC and MTP models as an additional refinement but is not deemed necessary here.

For MTP, a constant frequency shift of 22 cm^{-1} to the blue from the experimental spectra yielded the best overlap for the central −CO peak. The computations find a frequency of 1673 cm^{-1} for the central −CO (black), followed by the outer −CO at 1686 cm^{-1} (red), and finally the −CO(OH) group at 1739 cm^{-1} (green). Although the same force field (MTP and Morse) was used for the central and outer amide, the different environments experienced by them lead to a splitting of 13 cm^{-1}. This sensitivity to the environmental structure and dynamics is consistent with recent findings for insulin monomers and dimers.[8] Nevertheless, the experimentally observed splitting of 25 cm^{-1} is still underestimated.[31] The simulations with the PC model also yield the correct ordering for the frequencies of the central and outer −CO (at 1677, 1687 cm^{-1}), but the splitting is somewhat smaller (10 cm^{-1}) than that from the simulations using MTP. It is conceivable that further improvements of the electrostatics[64,65] lead to yet closer agreement between simulations and experiments. For one, conformationally dependent multipoles provide an even better description of the electrostatics as has been found for isolated CO in Mb.[66−69] Furthermore, including polarization may lead to additional improvements.

With SCC-DFTB, the central, outer, and terminal carbonyl peaks are at 1648, 1695, and 1598 cm^{-1} (Figure 5B,D). A constant frequency shift of 5 cm^{-1} (red) from the experimental spectra was considered to best overlap the central −CO peak for the simulations with the SCC-DFTB results. Consistent

https://doi.org/10.1021/acs.jpcb.1c05423
J. Phys. Chem. B 2021, 125, 10928−10938

Table 2. Parameters for Fitting the FFCFs to a Bi-exponential Decay with Static Component Fit (eq 3) for Trialanine from Simulations Using the PC, MTP, and SCC-DFTB Models

model	mode	a_1 [ps^{-2}]	τ_1 [ps]	a_2 [ps^{-2}]	τ_2 [ps]	Δ_0^2 [ps^{-2}]
MTP (FNM)	−CO(central)	1.348	0.038	0.274	1.337	0.723
	−CO (outer)	1.709	0.044	0.373	3.066	0.797
	−CO(OH)	1.804	0.067	0.568	3.184	0.620
MTP (INM)	−CO (central)	2.250	0.057	0.662	1.043	0.087
	−CO (outer)	2.360	0.076	0.419	1.543	0.023
PC (FNM)	−CO (central)	1.391	0.039	0.204	2.306	0.200
	−CO (outer)	1.942	0.037	0.422	4.697	0.419
	−CO(OH)	1.465	0.098	1.350	6.028	0.099
SCC-DFTB (FNM)	−CO (central)	4.872	0.076	3.052	1.845	0.908
	−CO (outer)	4.981	0.124	6.299	1.350	0.468
	−CO(OH)	9.780	0.311	9.198	3.508	2.877

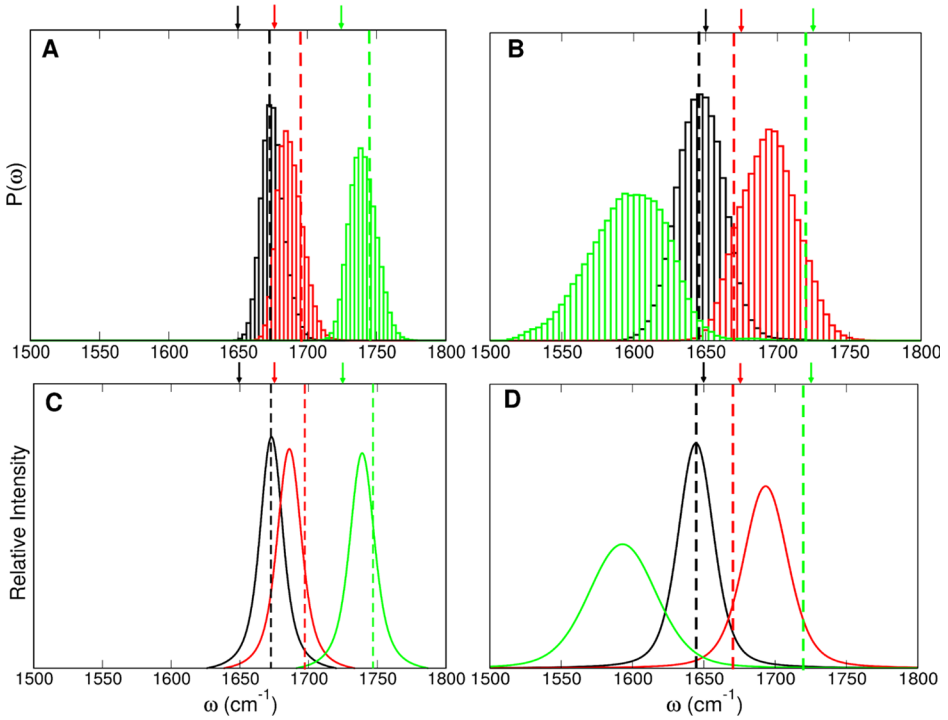

Figure 5. Frequency distributions (panels A,B) and 1D absorption spectra (panels C,D) of each −CO moiety of trialanine for the central (black), outer (red), and terminal (green) −CO. Panels (A,C) correspond to results using MTP, and panels (B,D) correspond to those from SCC-DFTB simulations. The down-headed arrows indicate the experimental[31] peak position of each −CO group, whereas the vertical dashed lines with corresponding color show the shifted experimental peak position to best overlap with the simulated data of central −CO. A constant shift of 22 cm^{-1} (blue) and 5 cm^{-1} (red) from the experimental spectra was considered to best overlap the central −CO peak for the simulations with MTPs and SCC-DFTB, respectively.

with the experiment, the frequency of the outer −CO is shifted to the blue (+47 cm^{-1}) from the central −CO by close to twice the value reported from the experiment (+25 cm^{-1}).[31] For the carboxylic (COOH) −CO, SCC-DFTB underestimates the frequency by 125 cm^{-1} compared with the experiment. This finding was reproduced from two independent simulations. Upon visual inspection of the trajectories, it was observed that the COOH unit is typically in an anti conformation, whereas the minimum energy structure is the syn conformer. To further validate the performance of SCC-DFTB, simulations for $(Ala)_3$ in the gas phase using the (second-order) mio[49,70] and (third-order) 3ob-freq[71] parameter sets were carried out. With the mio parameters, used for this study, the frequency distributions of the central and outer −CO label are split by ∼ 25 cm^{-1}—to be compared with a splitting of 25 cm^{-1} from the experiment in solution—whereas with the 3ob-freq parametrization—which was refined for thermochemistry, geometries, and vibrational frequencies in the gas phase—the splitting is 110 cm^{-1}. Hence, it is not expected that a different parametrization will appreciably improve the findings for simulations in solution.

Frequency Fluctuation Correlation Function. The FFCF provides information about the environmental dynamics surrounding a local spectroscopic probe and the coupling to it. The FFCFs were fitted to a bi-exponential decay with static component (eq 3) as has also been carried out for NMAD.[58] The raw data with the corresponding fits are shown in Figure 6, and the parameters are summarized in Table 2. FFCFs for each −CO probe of trialanine using the MTP model (Figure

https://doi.org/10.1021/acs.jpcb.1c05423
J. Phys. Chem. B 2021, 125, 10928−10938

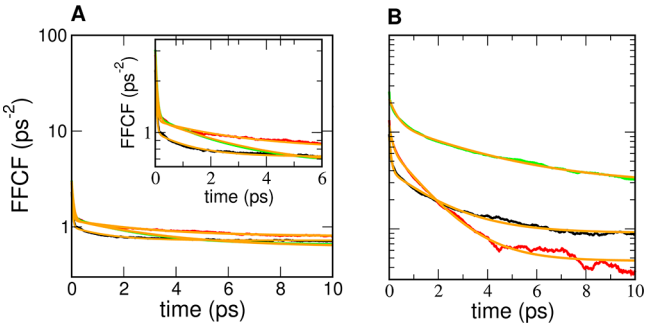

Figure 6. FFCF for each −CO moiety of trialanine using the MTP model (panel A) and from SCC-DFTB simulations (panel B) for central −CO (black), outer −CO (red), and the CO(OH) group (green). The orange lines are the fit to eq 3 for each case.

6A) and from SCC-DFTB simulations (Figure 6B) for central (black), outer (red), and terminal (green) −CO are reported.

The short time scale τ_1 ranges from 0.04 to 0.07 ps, whereas the longer one ranges from 1.3 to 3.2 ps. Using the PC simulations, the decay time τ_1 is similar to that from the MTP simulation, whereas the long time scales increase by about a factor of two. The amplitudes (a_1 and a_2) of the two time scales are comparable for the two methods. For the simulation with MTPs, the static components for the central and outer amide are similar in magnitude, on average $\Delta_0^2 \sim 0.75$ ps^{-2} (which yields $\Delta_0 \sim 0.866$ ps^{-1} equivalent to $\Delta_0 = 4.6$ cm^{-1}), which is in good agreement with the experimentally reported value[32] of $\Delta_0 = 5$ cm^{-1}. This static component appears for $(Ala)_3$ but not for NMA and is quantitatively captured by using the MTP force field together with the FNM analysis and consistent with the experiment which report that "In contrast to NMA, the amide-I band of trialanine is still notably inhomogeneous on the 4 ps time scale."[32] For the simulations with the PC model, the fits to eq 3 yield $\Delta_0^2 = 0.20$ ps^{-2} and $\Delta_0^2 = 0.42$ ps^{-2} which is smaller by about a factor of two compared with the experiment. Also, the two static components for the central and outer −CO label differ by a factor of two.

With SCC-DFTB, the short time decay τ_1 is considerably slower (0.1 ps to 0.3 ps) compared with the PC and MTP models, and the longer time scales range from 1.4 to 3.5 ps. The short time decay is considerably longer than that reported from the experiment, whereas the long time decay for the central and outer −CO are compatible with $\tau_c = 1.6$ ps used for interpreting experiments on $(Ala)_3$ which was, however, fixed at the value found for NMA.[32] The values of Δ_0^2 for the central and outer −CO differ by a factor of two, similar to the results from the simulations with PCs but on average, they are consistent with the experimental value.[32]

From experiments, the magnitude of $C(t = 0)$ (i.e., the FFCF at $t = 0$) has been reported to be $\Delta_1^2 = 121$ cm^{-2} equivalent to 4.30 ps^{-2}.[58] This compares with values of 1.65, 2.05, and 2.39 ps^{-2} from simulations with MTP and 8.5, 12.78, and 23.33 ps^{-2} from the SCC-DFTB simulations for the central, outer, and CO(OH) groups. Hence, the MTP simulations underestimate the experimentally reported amplitude, whereas SCC-DFTB simulations overestimate it by about a factor or two. This was also found for simulations and experiments on fluoro-acetonitrile.[61] The value $C(t = 0)$ is a measure of the interaction strength between the reporter(s) and the environment. Thus, the present findings suggest that this interaction is underestimated by the MTP model and overestimated by SCC-DFTB. Such information can be used to further improve the energy function.

Considering the results on the FFCFs for NMAD and $(Ala)_3$ together, it is noted that only the simulations with MTP are consistent with experiments in that (a) their decay times are close to one another and (b) the fact that the FFCF for NMAD has no static component but that for $(Ala)_3$ has $\Delta_0^2 > 0$. It is also of interest to note that the fast decay time $\tau_1 \lesssim 100$ fs of the FFCF observed in the present simulations is consistent with an experimentally observed time constant of $\tau = 110 \pm 20$ fs.[33]

The associated line shapes for the three different modes involving the −CO stretch for trialanine are calculated via 1D Fourier transformation of the line shape function as was done for NMAD, see Figure 5C,D. The fwhm for the 1D IR spectra is 13 cm^{-1} for the central −CO, 17 cm^{-1} for the outer one, and 18 cm^{-1} for the terminal −CO(OH) using the MTP model and 25, 32, and 50 cm^{-1} when using the SCC-DFTB model. Experimentally,[58] the fwhm for NMAD and $(Ala)_3$ differ little and are ∼20 cm^{-1}. Both findings are quite well captured by the MTP simulations, whereas with SCC-DFTB, the widths are larger and differ somewhat more between NMAD and $(Ala)_3$. The differences between the experimentally observed fwhm and those from the simulations are smaller than that for CN^- for which they differed by almost a factor of two[72] when rotational contributions to the line widths are neglected. It is possible that including such effects in the present case will further improve the agreement between simulations and experiments. However, due to the considerably smaller rotational constants of $(Ala)_3$ compared with CN^-, the effects will be less pronounced. Also, it is expected that simulations longer than 10 ns will not change these results appreciably because (a) the decay times of the FFCFs are shorter by at least 3 orders of magnitude and (b) recent convergence studies for amide-I spectroscopy on insulin monomers and dimers showed explicitly that such FFCFs are typically converged from simulations on the 5 ns time scale.[8] It is also possible that adjusting the nonbonded parameters further improves the fwhm. For example, the line shape from MTP simulations considerably broadens if the amplitudes from the FFCFs of the DFTB simulations are used. As the amplitude of the FFCF is a direct measure of the strength of the solute−solvent interaction, further improvements can be accomplished by modifying the −CO van der Waals parameters in the MTP model.

Structural Dynamics. To characterize the structural dynamics afforded by the different energy functions used in the present work, the distribution of Φ/Ψ angles (Ramachandran plot) were determined from trajectories with the PC, MTP, and SCC-DFTB models, see Figure 7. This is used to determine whether, depending on the energy function used, the conformational space sampled differs. Also, assessing differences in the sampling between simulations in the gas phase and in solution are of interest. Both, the conventional [Φ, Ψ] map for the central and outer −CO labels and the dihedral angles for the terminal −CO are reported.

Figure 7 shows the Ramachandran plot for trialanine from simulations using the PC (left panel), SCC-DFTB (middle panel), and MTP (right panel) models. The centers for the [Φ, Ψ] angles for the β, P_{II}, α_R, and α_L conformations are [−140°, 130°], [−75°, 150°], [−70°, −50°], and [50°, 50°], respectively. From simulations in the gas phase (top row), the

https://doi.org/10.1021/acs.jpcb.1c05423
J. Phys. Chem. B 2021, 125, 10928−10938

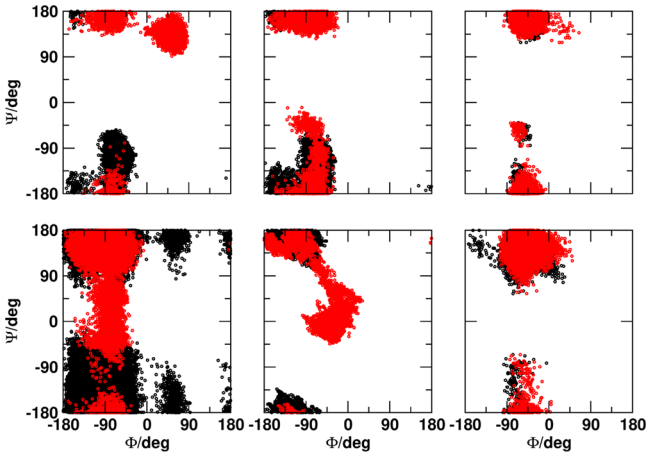

Figure 7. Ramachandran plots (Φ/Ψ angle) of trialanine using the PC (left panel), SCC-DFTB (middle panel), and MTP (right panel) models. Top and bottom panels are from simulations in the gas phase and in water, respectively. Black area denotes the Ramachandran angles, and red area denotes the Φ/Ψ angles of trialanine for the carboxylic terminus. The centers for the [Φ, Ψ] angles for the β, P_{II}, α_R, and α_L conformations are [−140°, 130°], [−75°, 150°], [−70°, −50°], and [50°, 50°], respectively.

distributions for the regular Ramachandran angles from PC and SCC-DFTB simulations are similar. They both sample β, P_{II}, and α_R structures. For simulations with MTP, the densities are somewhat more shifted toward the P_{II} structures, and the α_R state is sampled as well. For the COOH group (red), the region for Φ > 0 is occupied for simulations with PCs but not with SCC-DFTB and simulations with the MTP model sample the same regions as for the regular Ramachandran angles.

The distribution of conformational state population, as shown in Figure 7, finds increased flexibility of $(Ala)_3$ from simulations with the PC model compared with those using MTP and SCC-DFTB both in the gas phase and in water. For the simulations in water (bottom row in Figure 7), the changes compared with the gas phase are most pronounced with PCs. In addition to the β, P_{II}, and α_R structures, the poly-Gly regions are also accessed extensively. Contrary to that, the differences between the gas and the condensed phase from simulations with SCC-DFTB and MTP are smaller but nevertheless exhibit increased flexibility as was found for the simulations with PCs. Using SCC-DFTB, sampling of the β and P_{II} structures is extensive, whereas α_R is not sampled at all for the regular Ramachandran angle (but for the −COOH terminus, see red distribution). Finally, for MTP, the distributions in the region of the β and P_{II} states broaden, and there is also some limited sampling of the α_R helix. Both, SCC-DFTB and MTP only sample "allowed" regions in solution, whereas simulations with PCs also access "unusual" (poly-Gly) and "forbidden" regions.

Ramachandran maps have also been reported from simulations using a range of parametrized, PC-based force fields, including C27, C36, and C36m together with the TIP3P and SPC/E water models.[41] The distributions found in the present work, see Figure 7 (lower left panel), are consistent with these (Φ, Ψ) maps. Using a Bayesian refinement on the measured and computed 1D IR spectra, a consensus 2D potential of mean force (PMF) as a function of (Φ,Ψ) was determined. Notably, the refined PMF(Φ,Ψ) vis-a-vis experiment reported in ref 41 closely resembles the distribution found from the MTP simulations, see black symbols in Figure 7 (lower right panel).

Table 3 summarizes state populations for β, P_{II}, α_R, and α_L conformations of trialanine from simulations with PC, MTP, and SCC-DFTB models. A comparison with several previous studies is also provided.[31,34,36,37,39−41] For assigning a particular conformation to one of the four states, first centers (Φ and Ψ) of each of the states were defined as [−140°, 130°], [−75°, 150°], [−70°, −50°], and [50°, 50°] for β, P_{II}, α_R, and α_L conformations, respectively. If a particular conformation is within ±40° around any of the centers, the conformation is assigned to that center. If a conformation is outside these bounds, it is not assigned which is the case for 30 to 40% of the structures. Then, the percentage for the population of a particular substate was determined as the fraction of all assigned conformations. The present simulations using MTP find dominant population of the P_{II} state (98%) with a small fraction of β and α_R. Using a PC model, P_{II} is still most populated, followed by β and α_R. Simulations with SCC-DFTB yield a higher population of β, a smaller fraction for P_{II}, and no helical conformations.

Table 3. State Population for β, P_{II}, α_R, and α_L Conformations of Trialanine from Simulations with PC, MTP, and SCC-DFTB Compared with Previously Reported Values

	conformational state population			
	β	P_{II}	α_R	α_L
MTP (this work)	1%	98%	1%	0
PC (this work)	18%	79%	3%	<1%
SCC-DFTB (this work)	62%	38%	0	0
Tokmakoff et al. (original)[41a]	(22 ± 7)%	(63 ± 11)%	(12 ± 8)%	(3 ± 2)%
Tokmakoff et al. (Refined)[b]	(14 ± 5)%	(85 ± 6)%	(1 ± 2)%	<0.1%
Woutersen et al.,[31c]	0%	80%	20%	0%
Mu et al.[36]	42%	41%	16%	0.8%
Schweitzer-Stenner[34,d]	16%	84%	0%	0%
Graf et al.,[37e]	8%	92%	0%	0%
Oh et al.,[39f]	12%	88%	0%	0%
Xiao et al.,[40g]	2.0 ± 1.8)%	(85.8 ± 4.9)%	(5.5 ± 4.1)%	(3.5 ± 2.7)%
Beauchamp et al.,[73h]	(23 ± 6)%	(67 ± 9)%	(10 ± 8)%	

[a]MD simulation. [b]Bayesian ensemble refinement against FTIR and 2D IR. [c]Fitting 2D IR spectra. [d]Fitting vibrational circular dichroism, Raman, FTIR, and *J*-coupling. [e]Fitting NMR. [f]Fitting NMR with Gromos 43A1. [g]Fitting NMR with the integrated Bayesian approach. [h]Bayesian energy landscape tilting. The standard deviation from the average is given in parentheses.

https://doi.org/10.1021/acs.jpcb.1c05423
J. Phys. Chem. B 2021, 125, 10928−10938

Most previous studies find that the P_{II} state is most populated, typically followed by β structures. The relative populations range from 66 to 92% for P_{II} and 0 to 23% for β. Fewer studies report population of α_R. One of the most sophisticated investigations [Bayesian ensemble refinement against Fourier transform infrared (FTIR) and 2D IR experimental data][41] reports a (85 ± 6)% population for P_{II}, (14 ± 5)% for β, and an insignificant population (1 ± 2)% for α_R. Within error bars, the results from the MTP simulations are consistent with these findings. It is interesting to note that the "original" state populations in the work of Tokmakoff et al. were all derived from MD simulations using PC-based force fields, and the populations are largely independent on the particular choice of the all-atom FF, see Table S5 in ref 41. Specifically, the populations from the C36 parametrization with the TIP3P water model (as used here, see Table S4 in ref 41) are in agreement with the present findings for β structures (18% vs 20%), P_{II} (68% vs 79%), and α_R. (6% vs 3%). Differences may arise due to slightly different definitions of the basins to integrate the populations and whether or not all of the conformations are used for analysis. After Bayesian refinement, the populations are comparable to those from MTP simulations. In other words, machine learning of the populations based on the comparison of measured and computed IR spectra has the same effect as replacement of PCs by MTPs in the present simulations, lending additional support to the physical relevance afforded by the anisotropic effects in the electrostatic interactions.

FFCF from Independent NMs. The amide-I vibrational dynamics encoded in the FFCF contains information about the solvent dynamics and the peptide conformational dynamics. To better understand the influence of inter-mode couplings on the conformational dynamics, the instantaneous NMs for the central and the outer −CO label were also determined from NM analyses treating the two amide modes independently. This is then compared with the FFCFs obtained from FNM analysis which contains the couplings between the labels.

The FFCFs for the central and the outer −CO from INM (dashed lines) and from FNM (solid lines) are reported in Figure 8, and the fitting parameters to eq 3 using two time scales are given in Table 2. Without coupling (dashed lines), the FFCFs decay close to zero on the 10 ps time scale, and the magnitude of Δ_0^2 decreases by almost 1 order of magnitude compared with the results from FNM. Also, the decay times

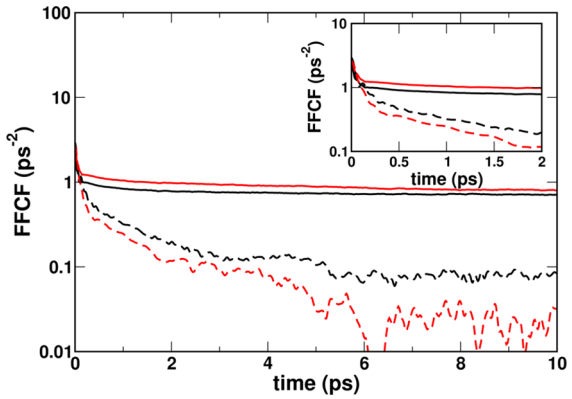

Figure 8. Comparison of FFCFs from full NM analysis (solid lines) and independent NM analysis (dashed lines) for the outer (red) and central (black) amide modes of trialanine.

are shorter if the coupling between the two labels is negligible. As the results from FNM analysis agree with the experiment and those omitting the coupling do not, it is concluded that the FNM analysis together with a MTP representation of the electrostatics provides a means to correctly describe the dynamics of hydrated $(Ala)_3$.

Including couplings between the labels ("sites") is also important when working with map-based approaches for 1D and 2D IR spectroscopies.[23,74,75] Using frequency maps, the site energies, the nearest neighbor coupling, and the transition dipole couplings are usually included in the excitonic Hamiltonian.[23] Such couplings need to be (re-)introduced in an excitonic Hamiltonian, but they are already partly present in the FNM approach used here, as the above analysis demonstrates. The MD simulations which generate the conformational ensemble to be analyzed include couplings through the nuclear dynamics, and FNM analysis preserves these couplings, whereas INM analysis almost entirely removes them.

Comparing the maxima of the peak positions from the frequency distributions based on "full NM" and "independent NM" reveals that the two analyses differ in capturing this coupling. From INM, the frequency distributions peak at 1661.5 cm^{-1} and 1662 cm^{-1}, that is, a splitting of close to zero, whereas from FNM, the maxima are at 1670 and 1683 cm^{-1}, that is, a splitting of 13 cm^{-1}. Within a simple two-state Hamiltonian, this amounts to a coupling of ∼6.5 cm^{-1}, consistent with experiments.[33]

The finite amplitude of Δ_0^2 is also indicative of the fact that within the explored time scale, the system has not exhaustively sampled all available states. In other words, population relaxation is not complete on the 10 ps time scale. This is consistent with an analysis of MD trajectories that determined the FFCF from only sampling the P_{II} conformation (which decays to zero on the ∼4 ps time scale) compared with the full MD trajectory sampling different substates for which a static contribution remains even after 10 ps.[58] This interpretation is also consistent with the fact that NMAD only has one conformational substate, and therefore, the FFCF decays to zero on the 10 ps time scale.

SUMMARY AND CONCLUSIONS

In summary, the present work provides a comprehensive assessment and comparison of the dynamics and IR spectroscopy of NMAD and $(Ala)_3$ in D_2O. Consistent with experiments on $(Ala)_3$, it is found that with "FNMs" from simulations using MTPs to compute the frequency trajectory, the 1D IR spectra for the outer and central −CO labels are split by 13 cm^{-1}, compared with 25 cm^{-1} from the experiment. With independent NMs, this splitting is close to zero. Including the site−site couplings in the NM analysis therefore yields a more quantitative description of the spectroscopy and dynamics. This splitting is larger (47 cm^{-1}) in simulations with SCC-DFTB for the solute. The FFCF from FNM has an initial amplitude $C(t = 0)$ of [1.65 and 2.05] ps^{-2} for the central and outer −CO label, compared with 4.30 ps^{-2} from the experiment and [8.50 and 12.78] ps^{-2} from simulations with SCC-DFTB. This points toward somewhat weaker interactions of the −CO labels with the environment in the MTP simulations and a considerably stronger interaction in the SCC-DFTB. The long-time static component from MTP simulations with FNM of Δ_0 = 4.6 cm^{-1} compares well with that observed experimentally (Δ_0 = 5.0 cm^{-1}), whereas that

https://doi.org/10.1021/acs.jpcb.1c05423
J. Phys. Chem. B 2021, 125, 10928−10938

from simulations with the PCs is smaller by a factor of two. The MTP simulations find comparable values for Δ_0 for the central and outer −CO, whereas with SCC-DFTB, they differ by about a factor of two with one of the values ∼ 20% larger than that observed experimentally and the other one lower by a similar amount, see Table 2.

Overall, simulations for $(Ala)_3$ with MTP and FNM analyses find good to quantitative agreement with experiments for the splitting, amplitude of $C(t = 0)$, and value for Δ_0. This contrasts with simulations using PC and/or INM or SCC-DFTB simulations. While for NMAD in D_2O, both PC- and MTP-based force fields were found to perform adequately:[24] the PC model for $(Ala)_3$ clearly is inferior to the MTP model as is evident when considering Δ_0 or the decay times for NMAD compared with $(Ala)_3$. The performance of SCC-DFTB could be improved by, for example, adjusting the van der Waals parameters which currently are those of the CHARMM force field or by using explicit H-bonding corrections.[76] The conformational space sampled by $(Ala)_3$ in solution is dominated by a P_{II} structure (98%), followed by β and α_R, each populated in 1% of the cases. This agrees qualitatively with a Bayesian refined analysis[41] of recent IR experiments which find occupations of (P_{II}, β, and α_R) and (85 ± 6, 14 ± 5, and 1 ± 2) % but differ somewhat from earlier results[31] which report (80, 0, and 20) %. Using MTP electrostatics on other spectroscopic probes is possible in general and has, in fact, already been used for NO attached to the sulfur of cysteine ("nitrosylation") to probe the structural dynamics and spectroscopy in myoglobin.[77]

The present work demonstrates that the structural dynamics of a small, hydrated peptide can be correctly described from MD simulations based on an MTP force field in explicit solvent together with FNM analysis. Such studies provide the necessary basis to link structural dynamics, spectroscopy, and aggregation in larger proteins from experiments and simulations.

■ ASSOCIATED CONTENT

Supporting Information

The Supporting Information is available free of charge at https://pubs.acs.org/doi/10.1021/acs.jpcb.1c05423.

Multipole parameters for the simulations of NMAD and $(Ala)_3$ (PDF)

■ AUTHOR INFORMATION

Corresponding Authors

Padmabati Mondal − *Department of Chemistry, University of Basel, Basel 4056, Switzerland;* Present Address: Department of Chemistry and Center for Atomic, Molecular and Optical Sciences and Technologies, Indian Institute of Science Education and Research (IISER) Tirupati, Karakambadi Road, Mangalam, Tirupati-517507, Andhra Pradesh, India; orcid.org/0000-0003-1523-630X; Email: padmabati.mondal@iisertirupati.ac.in

Markus Meuwly − *Department of Chemistry, University of Basel, Basel 4056, Switzerland; Department of Chemistry, Brown University, Providence/RI 02912, United States;* orcid.org/0000-0001-7930-8806; Email: m.meuwly@unibas.ch

Authors

Pierre-André Cazade − *Department of Chemistry, University of Basel, Basel 4056, Switzerland;* Present Address: Bernal Institute, University of Limerick, Plassey Park Road, co. Limerick, V94 T9PX, Ireland.; orcid.org/0000-0002-6860-4658

Akshaya K. Das − *Department of Chemistry, University of Basel, Basel 4056, Switzerland;* Present Address: Pitzer Theory Center, University of California,260, Stanley Hall, Berkeley, CA 94720-3220.

Tristan Bereau − *Department of Chemistry, University of Basel, Basel 4056, Switzerland;* Present Address: Van 't Hoff Institute for Molecular Sciences and Informatics Institute, University of Amsterdam, Amsterdam 1098 XH, The Netherlands and Max-Planck-Institut für Polymerforschung, Ackermannweg 10, 55128 Mainz, Germany.; orcid.org/0000-0001-9945-1271

Complete contact information is available at: https://pubs.acs.org/10.1021/acs.jpcb.1c05423

Notes

The authors declare no competing financial interest.

■ ACKNOWLEDGMENTS

The authors gratefully acknowledge financial support from the Swiss National Science Foundation through grant 200021-117810 and to the NCCR-MUST. The authors thank Prof. Peter Hamm for valuable discussions. P.M. acknowledges DST, SERB, GoI (SRG/2020/001354) for financial support.

■ REFERENCES

(1) Ganim, Z.; Chung, H. S.; Smith, A. W.; DeFlores, L. P.; Jones, K. C.; Tokmakoff, A. Amide I two dimensional infrared spectroscopy of proteins. *Acc. Chem. Res.* **2008**, *41*, 432.

(2) Getahun, Z.; Huang, C.-Y.; Wang, T.; De León, B.; DeGrado, W. F.; Gai, F. Using Nitrile-Derivatized Amino Acids as Infrared Probes of Local Environment. *J. Am. Chem. Soc.* **2003**, *125*, 405−411.

(3) Bagchi, S.; Boxer, S. G.; Fayer, M. D. Ribonuclease S Dynamics Measured Using a Nitrile Label with 2D IR Vibrational Echo Spectroscopy. *J. Phys. Chem. B* **2012**, *116*, 4034−4042.

(4) Xu, L.; Cohen, A. E.; Boxer, S. G. Electrostatic Fields near the Active Site of Human Aldose Reductase:2. New Inhibitors and Complications Caused by Hydrogen Bonds. *Biochem* **2011**, *50*, 8311−8322.

(5) Mondal, P.; Meuwly, M. Vibrational Stark Spectroscopy for Assessing Ligand-Binding Strength in a Protein. *Phys. Chem. Chem. Phys.* **2017**, *19*, 16131−16143.

(6) Bloem, R.; Koziol, K.; Waldauer, S. A.; Buchli, B.; Walser, R.; Samatanga, B.; Jelesarov, I.; Hamm, P. Ligand Binding Studied by 2D IR Spectroscopy Using the Azidohomoalanine Label. *J. Phys. Chem. B* **2012**, *116*, 13705−13712.

(7) Layfield, J. P.; Hammes-Schiffer, S. Calculation of Vibrational Shifts of Nitrile Probe in the Active Site of Ketosteroid Isomerase upon Ligand Binding. *J. Am. Chem. Soc.* **2013**, *135*, 717−725.

(8) Salehi, S. M.; Koner, D.; Meuwly, M. Dynamics and Infrared Spectroscopy of Monomeric and Dimeric Wild Type and Mutant Insulin. *J. Phys. Chem. B* **2020**, *124*, 11882−11894.

(9) Waegele, M. M.; Culik, R. M.; Gai, F. Site-Specific Spectroscopic Reporters of the Local Electric Field, Hydration, Structure, and Dynamics of Biomolecules. *J. Phys. Chem. Lett.* **2011**, *2*, 2598−2609.

(10) Koziol, K. L.; Johnson, P. J.; Stucki-Buchli, B.; Waldauer, S. A.; Hamm, P. Fast infrared spectroscopy of protein dynamics: advancing sensitivity and selectivity. *Curr. Opin. Struct. Biol.* **2015**, *34*, 1−6.

(11) Horness, R. E.; Basom, E. J.; Thielges, M. C. Site-selective characterization of Src homology 3 domain molecular recognition

with cyanophenylalanine infrared probes. *Anal. Chem.* **2015**, *7*, 7234−7241.
(12) Getahun, Z.; Huang, C.-Y.; Wang, T.; De León, B.; DeGrado, W. F.; Gai, F. Using nitrile-derivatized amino acids as infrared probes of local environment. *J. Am. Chem. Soc.* **2003**, *125*, 405−411.
(13) Kozinski, M.; Garrett-Roe, S.; Hamm, P. 2D-IR spectroscopy of the sulfhydryl band of cysteines in the hydrophobic core of proteins. *J. Phys. Chem. B* **2008**, *112*, 7645−7650.
(14) Zimmermann, J.; Thielges, M. C.; Yu, W.; Dawson, P. E.; Romesberg, F. E. Carbon-Deuterium Bonds as Site-Specific and Nonperturbative Probes for Time-Resolved Studies of Protein Dynamics and Folding. *J. Phys. Chem. Lett.* **2011**, *2*, 412−416.
(15) Woys, A. M.; Mukherjee, S. S.; Skoff, D. R.; Moran, S. D.; Zanni, M. T. A Strongly Absorbing Class of Non-Natural Labels for Probing Protein Electrostatics and Solvation with FTIR and 2D IR Spectroscopies. *J. Phys. Chem. B* **2013**, *117*, 5009−5018.
(16) Zimmermann, J.; Thielges, M. C.; Seo, Y. J.; Dawson, P. E.; Romesberg, F. E. Cyano Groups as Probes of Protein Microenvironments and Dynamics. *Angew. Chem., Int. Ed.* **2011**, *50*, 8333−8337.
(17) van Wilderen, L. J. G. W.; Kern-Michler, D.; Müller-Werkmeister, H. M.; Bredenbeck, J. Vibrational dynamics and solvatochromism of the label SCN in various solvents and hemoglobin by time dependent IR and 2D-IR spectroscopy. *Phys. Chem. Chem. Phys.* **2014**, *16*, 19643−19653.
(18) Lee, G.; Kossowska, D.; Lim, J.; Kim, S.; Han, H.; Kwak, K.; Cho, M. Cyanamide as an Infrared Reporter: Comparison of Vibrational Properties between Nitriles Bonded to N and C Atoms. *J. Phys. Chem. B* **2018**, *122*, 4035−4044.
(19) Hamm, P.; Zanni, M. *Concept and Methods of 2D Infrared Spectroscopy*; Cambridge University Press, 2011.
(20) Hamm, P.; Lim, M.; Hochstrasser, R. M. Structure of the Amide I Band of Peptides Measured by Femtosecond Nonlinear-Infrared Spectroscopy. *J. Phys. Chem. B* **1998**, *102*, 6123−6138.
(21) Zanni, M. T.; Asplund, M. C.; Hochstrasser, R. M. Two Dimensional Heterodyned and Stimulated Infrared Photon Echoes of N-Methylacetamide-D. *J. Chem. Phys.* **2001**, *114*, 4579−4590.
(22) Woutersen, S.; Mu, Y.; Stock, G.; Hamm, P. Hydrogen-bond lifetime measured by time-resolved 2D-IR spectroscopy: N-methylacetamide in methanol. *Chem. Phys.* **2001**, *266*, 137−147.
(23) Wang, L.; Middleton, C. T.; Zanni, M. T.; Skinner, J. L. Development and Validation of Transferable Amide I Vibrational Frequency Maps for Peptides. *J. Phys. Chem. B* **2011**, *115*, 3713−3724.
(24) Cazade, P.-A.; Bereau, T.; Meuwly, M. Computational Two-Dimensional Infrared Spectroscopy without Maps: N-Methylacetamide in Water. *J. Phys. Chem. B* **2014**, *118*, 8135−8147.
(25) Yadav, V. K.; Chandra, A. First-Principles Simulation Study of Vibrational Spectral Diffusion and Hydrogen Bond Fluctuations in Aqueous Solution of N-Methylacetamide. *J. Phys. Chem. B* **2015**, *119*, 9858−9867.
(26) Gaigeot, M. P.; Vuilleumier, R.; Sprik, M.; Borgis, D. Infrared Spectroscopy of N-Methylacetamide Revisited by ab initio Molecular Dynamics Simulations. *J. Chem. Theory Comput.* **2005**, *1*, 772−789.
(27) Cazade, P.-A.; Meuwly, M. Oxygen Migration Pathways in NO-bound Truncated Hemoglobin. *ChemPhysChem* **2012**, *13*, 4276−4286.
(28) Cho, M.; Fleming, G. R.; Saito, S.; Ohmine, I.; Stratt, R. M. Instantaneous normal mode analysis of liquid water. *J. Chem. Phys.* **1994**, *100*, 6672−6683.
(29) Salehi, S. M.; Koner, D.; Meuwly, M. Vibrational Spectroscopy of in the Gas and Condensed Phase. *J. Phys. Chem. B* **2019**, *123*, 3282−3290.
(30) Koner, D.; Salehi, M.; Mondal, P.; Meuwly, M. Non-conventional Force Fields for Applications in Spectroscopy and Chemical Reaction Dynamics. *J. Chem. Phys.* **2020**, *153*, 10901.
(31) Woutersen, S.; Hamm, P. Structure Determination of Trialanine in Water Using Polarization Sensitive Two-Dimensional Vibrational Spectroscopy. *J. Phys. Chem. B* **2000**, *104*, 11316−11320.
(32) Woutersen, S.; Pfister, R.; Hamm, P.; Mu, Y.; Kosov, D. S.; Stock, G. Peptide Conformational Heterogeneity Revealed from Nonlinear Vibrational Spectroscopy and Molecular-Dynamics Simulations. *J. Chem. Phys.* **2002**, *117*, 6833−6840.
(33) Woutersen, S.; Mu, Y.; Stock, G.; Hamm, P. Subpicosecond conformational dynamics of small peptides probed by two-dimensional vibrational spectroscopy. *Proc. Natl. Acad. Sci. U.S.A.* **2001**, *98*, 11254−11258.
(34) Schweitzer-Stenner, R.; Eker, F.; Huang, Q.; Griebenow, K. Dihedral Angles of Trialanine in D_2O Determined by Combining FTIR and Polarized Visible Raman Spectroscopy. *J. Am. Chem. Soc.* **2001**, *123*, 9628−9633.
(35) Woutersen, S.; Hamm, P. Isotope-edited two-dimensional vibrational spectroscopy of trialanine in aqueous solution. *J. Chem. Phys.* **2001**, *114*, 2727.
(36) Mu, Y.; Stock, G. Conformational Dynamics of Trialanine in Water : A Molecular Dynamical Study. *J. Phys. Chem. B* **2002**, *106*, 5294−5301.
(37) Graf, J.; Nguyen, P. H.; Schwalbe, H. Structure and dynamics of the homologous series of alanine peptides: a joint molecular dynamics/NMR study. *J. Am. Chem. Soc.* **2007**, *129*, 1179−1189.
(38) Gorbunov, R. D.; Nguyen, P. H.; Kobus, M.; Stock, G. Quantum-classical description of the amide I vibrational spectrum of trialanine. *J. Chem. Phys.* **2007**, *126*, 054509−054516.
(39) Oh, K. I.; Lee, K. K.; Cho, M. Circular dichroism eigen spectra of polyproline II and β-strand conformers of trialanine in water: singular value decomposition analysis. *Chirality* **2010**, *22*, E186−E201.
(40) Xiao, X.; Kallenbach, N.; Zhang, Y. Peptide conformation analysis using an integrated Bayesian approach. *J. Chem. Theory Comput.* **2014**, *10*, 4152−4159.
(41) Feng, C. J.; Dhayalan, B.; Tokmakoff, A. Refinement of Peptide Conformational Ensemblesby 2D IR Spectroscopy: Application to Ala-Ala-Ala. *Biophys. J.* **2018**, *114*, 2820−2832.
(42) Jorgensen, W. L.; Chandrasekhar, J.; Madura, J. D.; Impey, R. W.; Klein, M. L. Comparison of Simple Potential Functions for Simulating Liquid Water. *J. Chem. Phys.* **1983**, *79*, 926−935.
(43) Brooks, B. R.; Brooks, C. L., III; Mackerell, A. D., Jr.; Nilsson, L.; Petrella, R. J.; Roux, B.; Won, Y.; Archontis, G.; Bartels, C.; Boresch, S.; et al. CHARMM: The Biomolecular Simulation Program. *J. Comput. Chem.* **2009**, *30*, 1545−1614.
(44) Bereau, T.; Kramer, C.; Meuwly, M. Leveraging Symmetries of Static Atomic Multipole Electrostatics in Molecular Dynamics Simulations. *J. Chem. Theory Comput.* **2013**, *9*, 5450−5459.
(45) Kramer, C.; Gedeck, P.; Meuwly, M. Atomic Multipoles: Electrostatic Potential Fit, Local Reference Axis Systems and Conformational Dependence. *J. Comput. Chem.* **2012**, *33*, 1673−1688.
(46) Vanommeslaeghe, K.; Hatcher, E.; Acharya, C.; Kundu, S.; Zhong, S.; Shim, J.; Darian, E.; Guvench, O.; Lopes, P.; Vorobyov, I.; et al. CHARMM General Force Field: A Force Field for Drug-Like Molecules Compatible with the CHARMM All-Atom Additive Biological Force Fields. *J. Comput. Chem.* **2010**, *31*, 671−690.
(47) Darden, T.; York, D.; Pedersen, L. Particle mesh Ewald: An Nlog(N) method for Ewald sums in large systems. *J. Phys. Chem. B* **1993**, *98*, 10089−10096.
(48) van Gunsteren, W.; Berendsen, H. Algorithms for Macromolecular Dynamics and Constraint Dynamics. *Mol. Phys.* **1977**, *34*, 1311−1327.
(49) Elstner, M.; Porezag, D.; Jungnickel, G.; Elsner, J.; Haugk, M.; Frauenheim, T.; Suhai, S.; Seifert, G. Self-consistent-charge density-functional tight-binding method for simulations of complex materials properties. *Phys. Rev. B* **1998**, *58*, 7260−7268.
(50) Cui, Q.; Elstner, M.; Kaxiras, E.; Frauenheim, T.; Karplus, M. A QM/MM Implementation of the Self-Consistent Charge Density Functional Tight Binding (SCC-DFTB) Method. *J. Phys. Chem. B* **2001**, *105*, 569−585.
(51) Vanommeslaeghe, K.; Hatcher, E.; Acharya, C.; Kundu, S.; Zhong, S.; Shim, J.; Darian, E.; Guvench, O.; Lopes, P.; Vorobyov, I.;

et al. CHARMM General Force Field (CGenFF): A force field for drug-like molecules compatible with the CHARMM all-atom additive biological force fields. *J. Comput. Chem.* **2010**, *31*, 671−690.
(52) Salehi, S. M.; Meuwly, M. Site-Selective Dynamics of Azidolysozyme. **2021**, arXiv:2102.06545. arXiv preprint.
(53) Adams, J. E.; Stratt, R. M. Instantaneous Normal Mode Analysis as a Probe of Cluster Dynamics. *J. Chem. Phys.* **1990**, *93*, 1332−1346.
(54) Buchner, M.; Ladanyi, B. M.; Stratt, R. M. The Short-Time Dynamics of Molecular Liquids-Instantaneous-Normal-Mode Theory. *J. Chem. Phys.* **1992**, *97*, 8522−8535.
(55) Bastida, A.; Soler, M. A.; Zuniga, J.; Requena, A.; Kalstein, A.; Fernandez-Alberti, S. Instantaneous normal modes, resonances, and decay channels in the vibrational relaxation of the amide I mode of N-methylacetamide-D in liquid deuterated water. *J. Chem. Phys.* **2010**, *132*, 224501.
(56) Sun, X.; Stratt, R. M. How a solute-pump/solvent-probe spectroscopy can reveal structural dynamics: Polarizability response spectra as a two-dimensional solvation spectroscopy. *J. Chem. Phys.* **2013**, *139*, 044506.
(57) Schmidt, J.; Roberts, S.; Loparo, J.; Tokmakoff, A.; Fayer, M.; Skinner, J. Are water simulation models consistent with steady-state and ultrafast vibrational spectroscopy experiments? *Chem. Phys.* **2007**, *341*, 143−157.
(58) Woutersen, S.; Pfister, R.; Hamm, P.; Mu, Y.; Kosov, D.; Stock, G. Peptide conformational heterogeneity revealed from nonlinear vibrational spectroscopy and molecular-dynamics simulations. *J. Chem. Phys.* **2002**, *117*, 6833−6840.
(59) Decamp, M. F.; Deflores, L.; Mccracken, J. M.; Tokmakoff, A.; Kwac, K.; Cho, M. Amide I Vibrational Dynamics of N-Methylacetamide in Polar Solvents: The Role of Electrostatic Interaction. *J. Phys. Chem. B* **2005**, *109*, 11016−11026.
(60) Laage, D.; Stirnemann, G.; Sterpone, F.; Rey, R.; Hynes, J. T. Reorientation and allied dynamics in water and aqueous solutions. *Annu. Rev. Phys. Chem.* **2011**, *62*, 395−416.
(61) Cazade, P. A.; Tran, H.; Bereau, T.; Das, A. K.; Kläsi, F.; Hamm, P.; Meuwly, M. Solvation of fluoro-acetonitrile in water by 2D-IR spectroscopy : A combined experimental-computational study. *J. Chem. Phys.* **2015**, *142*, 212415−212424.
(62) Kubelka, J.; Keiderling, T. Ab Initio Calculation of Amide Carbonyl Stretch Vibrational Frequencies in Solution with Modified Basis Sets. 1. N-methyl Acetamide. *J. Phys. Chem. A* **2001**, *105*, 10922−10928.
(63) Jones, R. L. The infrared spectra of some simple N-substituted amides in the vapor state. *J. Mol. Spectrosc.* **1963**, *11*, 411−421.
(64) Devereux, M.; Raghunathan, S.; Fedorov, D. G.; Meuwly, M. A novel, computationally efficient multipolar model employing distributed charges for molecular dynamics simulations. *J. Chem. Theory Comput.* **2014**, *10*, 4229−4241.
(65) Unke, O. T.; Devereux, M.; Meuwly, M. Minimal distributed charges: Multipolar quality at the cost of point charge electrostatics. *J. Chem. Phys.* **2017**, *147*, 161712.
(66) Nutt, D. R.; Meuwly, M. Theoretical investigation of infrared spectra and pocket dynamics of photodissociated carbonmonoxy myoglobin. *Biophys. J.* **2003**, *85*, 3612−3623.
(67) Nutt, D. R.; Meuwly, M. Migration in native and mutant myoglobin: Atomistic simulations for the understanding of protein function. *Proc. Natl. Acad. Sci. U.S.A.* **2004**, *101*, 5998−6002.
(68) Plattner, N.; Meuwly, M. Higher order multipole moments for molecular dynamics simulations. *J. Mol. Model.* **2009**, *15*, 687−694.
(69) Plattner, N.; Meuwly, M. The role of higher CO-multipole moments in understanding the dynamics of photodissociated carbonmonoxide in myoglobin. *Biophys. J.* **2008**, *94*, 2505−2515.
(70) Krüger, T.; Elstner, M.; Schiffels, P.; Frauenheim, T. Validation of the density-functional based tight-binding approximation method for the calculation of reaction energies and other data. *J. Chem. Phys.* **2005**, *122*, 114110.
(71) Gaus, M.; Goez, A.; Elstner, M. Parametrization and benchmark of DFTB3 for organic molecules. *J. Chem. Theory Comput.* **2013**, *9*, 338−354.
(72) Lee, M. W.; Carr, J. K.; Göllner, M.; Hamm, P.; Meuwly, M. 2D IR Spectra of Cyanide in Water Investigated by Molecular Dynamics Simulations. *J. Chem. Phys.* **2013**, *139*, 054506.
(73) Beauchamp, K. A.; Pande, V. S.; Das, R. Bayesian energy landscape tilting: towards concordant models of molecular ensembles. *Biophys. J.* **2014**, *106*, 1381−1390.
(74) Jansen, T. l. C.; Dijkstra, A. G.; Watson, T. M.; Hirst, J. D.; Knoester, J. Modeling the amide I bands of small peptides. *J. Chem. Phys.* **2006**, *125*, 044312.
(75) Reppert, M.; Tokmakoff, A. Electrostatic frequency shifts in amide I vibrational spectra: Direct parameterization against experiment. *J. Chem. Phys.* **2013**, *138*, 134116.
(76) Rezac, J. Empirical self-consistent correction for the description of hydrogen bonds in DFTB3. *J. Chem. Theory Comput.* **2017**, *13*, 4804−4817.
(77) Turan, H. T.; Meuwly, M. Spectroscopy, dynamics, and hydration of S-nitrosylated myoglobin. *J. Phys. Chem. B* **2021**, *125*, 4262−4273.

https://doi.org/10.1021/acs.jpcb.1c05423
J. Phys. Chem. B 2021, 125, 10928−10938